Food and Bioprocess Technology (2026) 19:191
https://doi.org/10.1007/s11947-026-04284-3

RESEARCH

Physicochemical, Structural, and Techno-functional Characterization of *Solanum scabrum* Leaf Protein Concentrates Obtained by Alkaline Extraction, Ultrasound-assisted Extraction, and Ultrafiltration

Mary Nkongho Tanyitiku[1,2] · Shiksha Chaturvedi[1] · Rakshya Pandit[1] · Komalpreet[1] · Jyothi Dasari[1] · Aparna Philipose Antony[1]

Received: 9 January 2026 / Accepted: 17 February 2026

Abstract
Global demand for plant-based proteins is rapidly increasing, driven by sustainability concerns and health-conscious consumer preferences. In this context, African nightshade (*Solanum scabrum*), an underutilized leafy biomass rich in protein, represents a promising alternative protein source. This study investigated the influence of alkaline extraction followed by isoelectric precipitation (AE-IP), ultrasound-assisted extraction (UAE), and ultrafiltration (UF), on the yield, composition, structural and functional characteristics of *Solanum scabrum* protein concentrates (AE-IP_SPC, UAE_SPC, UF_SPC). UAE significantly enhanced protein yield (48.71%) compared to AE-IP (34.02%), while UF produced concentrates with lowest yield (26.45%) but highest protein content (71.43%). UF_SPC exhibited a lighter color ($L^* = 71.53 \pm 0.22$) and lower browning index ($20.76 \pm 0.11\%$) than AE-IP_SPC ($L^* = 57.89 \pm 0.17$; browning index $= 42.90 \pm 0.54\%$), indicating reduced pigment co-extraction. Scanning electron microscopy revealed dense, fibrous structures with irregular cracks in AE-IP_SPC, smooth, layered structures with interconnected channels and cavities in UAE_SPC, and irregular wavy patterns and shallow depressions in UF_SPC. UF_SPC displayed the highest absolute zeta potential values at both acidic (36 mV at pH 2) and alkaline pH (-39 mV at pH 10), indicating enhanced electrostatic repulsion and improved colloidal stability. Functionally, UF_SPC and UAE_SPC exhibited superior solubility at alkaline pH, along with enhanced emulsifying and foaming properties. Spectroscopic analysis suggested extraction-dependent alterations in protein conformation associated with improved hydration behavior. Overall, ultrasound-assisted and ultrafiltration approaches effectively improved the functional and nutritional performance of *Solanum scabrum* protein concentrates, supporting their potential application as sustainable plant-based protein ingredients and establishing clear process-structure–function relationships.

Keywords *Solanum scabrum* · Plant-based proteins · Ultrasound-assisted extraction · Ultrafiltration · Techno-functional properties · Sustainable food ingredients

Introduction

The global demand for protein is projected to increase substantially by 2050, driven by population growth, urbanization, and a transition toward sustainable dietary patterns (Gasparre et al., 2025). Meeting this demand is challenging since conventional animal protein production remains resource-intensive and environmentally detrimental (Ismail et al., 2020). Within this context, plant-based proteins have emerged as a viable solution, offering reduced environmental impact and desirable techno-functional properties such as emulsification, foaming, and gelation (Gasparre et al., 2025; Illingworth et al., 2024; Vogelsang-O'Dwyer et al., 2023). Although plant proteins may exhibit limitations in certain essential amino acids, they often contain elevated levels of amino acids including glutamic acid, aspartic acid, and arginine, that confer nutritional and functional benefits (Qin et al., 2022; Vogelsang-O'Dwyer et al., 2023). The global plant-based protein market, valued at USD 38 billion

✉ Mary Nkongho Tanyitiku
Mary.Tanyitiku@greenwich.ac.uk

[1] Food and Markets Department, Natural Resources Institute, University of Greenwich, Chatham Maritime, Kent ME4 4TB, UK

[2] Medway Food Innovation Centre, Natural Resources Institute, University of Greenwich, Chatham Maritime, Kent ME4 4TB, UK

Published online: 25 February 2026

in 2019, is anticipated to grow at an annual rate of 9.1% through 2027 (Ismail et al., 2020). Consequently, the identification and utilization of novel and underexploited plant protein sources have become a strategic priority for developing resilient and sustainable food systems (Cheng et al., 2021; Muller et al., 2024; Pérez-Vila et al., 2022).

African nightshade (*Solanum scabrum*) is increasingly recognized as a nutrient-dense, climate-resilient crop with considerable potential to enhance food and nutrition security (Kirigia et al., 2019; Lugumira et al., 2025). Its leaves are rich in essential nutrients, including high-quality protein (22.9–35.0%) with balanced levels of essential amino acids, dietary fiber (1.6–8.7%), vitamins (A, C, and E), minerals (such as iron and calcium), phenolics and flavonoids (Lugumira et al., 2025; Njong et al., 2023; Odongo et al., 2021). Despite its long history of consumption as a leafy vegetable, *S. scabrum* remains underexploited beyond traditional household use, particularly in sub-Saharan Africa where it grows abundantly (Kirigia et al., 2019; Odongo et al., 2021). Research on *S. scabrum* have largely focused on its phytochemical properties (Bando et al., 2025; Bayang et al., 2025; Kirigia et al., 2019; Lugumira et al., 2025; Njong et al., 2023; Odongo et al., 2021). However, its potential as a plant-based protein source for developing value-added food ingredients remains underexplored.

Previous studies have demonstrated that extraction treatments can induce significant structural and functional modifications in leaf proteins, including reductions in particle size, alterations in secondary structure, and changes in solubility, emulsifying, and gelation behavior (Cheng et al., 2021; Huang et al., 2024; Ismail et al., 2020; Pérez-Vila et al., 2022; Yang et al., 2024), Conventional alkaline extraction followed by isoelectric precipitation (AE-IP) is widely applied to plant biomasses due to its simplicity and relatively high recovery yield; however, it often promotes extensive protein unfolding, aggregation, and non-specific co-extraction of non-protein components, which may compromise functionality and purity (Anuar & Zuo, 2025; Furia et al., 2025; Pérez-Vila et al., 2022). Emerging approaches such as ultrasound-assisted extraction (UAE) enhance mass transfer through acoustic cavitation, improving protein release and potentially modifying functional attributes with reduced chemical severity (Yang et al., 2024). In contrast, ultrafiltration (UF) is a membrane-based concentration and fractionation technique that selectively retains protein macromolecules while removing low-molecular-weight solutes, thereby offering a milder route that may better preserve native structure and interfacial functionality (Huang et al., 2024; John et al., 2024). Despite increasing interest in alternative extraction strategies for leafy proteins (Anuar & Zuo, 2025; Kadam et al., 2015; Khan et al., 2024; Zheng et al., 2019), comparative evaluations of AE-IP, UAE, and UF applied specifically to *Solanum scabrum* remain scarce.

Therefore, this study systematically examined the influence of these three protein recovery strategies on yield, structural characteristics, and techno-functional performance of *S. scabrum* leaf protein concentrates, with the aim of elucidating process-structure–function relationships relevant to their application in structured and protein-enriched food systems.

Materials and Methods

Materials

Fresh leaves of African nightshade (*Solanum scabrum* Mill.) were obtained in July 2024 from a local farm in Ahala, Yaoundé III, Centre region, Cameroon. They were harvested at day 65 after planting as this period was found to be the most rich in bioactive compounds (Kirigia et al., 2019; Odongo et al., 2021). The leaves were manually sorted, destalked and thoroughly washed with deionised water to remove surface impurities. They were drained and crushed using an immersion blender (Breville, Australia; cutting speed, 30–40 mm/s; sharpening angle of the blade, 45°, and crushing time, 5–10 s). The crushed leaves were then frozen at −18℃ for 24 h and dried using a domestic freeze dryer (Harvest Right, United States), set at −50℃ for 48 h. The dry leaves were then ground and sieved using an ASTM E11 400 µm stainless steel to obtain *S. scabrum* leaf powder (SLP). The crude protein content of SLP is reported in Table 1. SLP was then stored in airtight polyethylene bags during analysis. Unless otherwise stated, all chemicals and reagents were obtained from Merck Life Science (Sigma-Aldrich brand, Gillingham, United Kingdom) and were of analytical grade.

Extraction and Concentration Methods

Alkaline Extraction

Alkaline extraction (AE-IP) was carried out according to Rezvankhah et al. (2021) with slight modifications. *S. scabrum* leaf powder (SLP) was dispersed in deionised water at a solid–liquid ratio of 1:20 (w/v), and the pH of the suspension was adjusted to 9.0 using 0.1 M NaOH to promote protein solubilisation prior to recovery. The alkaline leaf suspension (pH 9.0) was stirred continuously at room temperature (25 ± 2℃) for 1 h to promote protein solubilisation. The suspension was then centrifuged (Heraeus Megafuge 8 centrifuge, Thermo Scientific, United Kingdom) at 5,000 × g for 40 min at 4℃. The process was repeated three times and the supernatants (clarified alkaline extract) containing solubilised proteins was collected, and the pH was adjusted to 4.5 using 0.1 M HCl to induce isoelectric precipitation. This was then allowed to stand for 30 min to facilitate protein

Table 1 Composition and protein yield of *S. scabrum* leaf powder and protein concentrates

Macro-nutrients	SLP	AE-IP_SPC	UAE_SPC	UF_SPC
Protein yield (%)	-	34.02 ± 0.80^{b}	48.71 ± 0.42^{a}	26.45 ± 0.51^{c}
Moisture (g/100 g)	7.09 ± 0.61^{a}	5.53 ± 0.21^{b}	6.91 ± 0.34^{a}	5.62 ± 0.31^{b}
Ash (g/100 g)	13.76 ± 0.64^{a}	7.63 ± 0.81^{b}	6.62 ± 0.18^{c}	4.53 ± 0.22^{d}
Protein (g/100 g)	31.54 ± 0.70^{d}	68.73 ± 0.51^{b}	61.65 ± 0.11^{c}	71.43 ± 0.66^{a}
Fats (g/100 g)	2.54 ± 0.55^{a}	2.03 ± 0.24^{a}	1.86 ± 0.25^{a}	1.12 ± 0.40^{b}
Starch (g/100 g)	2.30 ± 0.04^{a}	0.49 ± 0.22^{b}	0.27 ± 0.40^{b}	0.15 ± 0.04^{c}
Soluble fibre (g/100 g)	5.80 ± 0.32^{a}	2.34 ± 0.17^{b}	1.89 ± 0.75^{b}	0.87 ± 0.72^{c}
Insoluble fibre (g/100 g)	8.82 ± 0.32^{a}	5.64 ± 0.04^{b}	6.32 ± 0.80^{b}	2.44 ± 0.08^{c}
Total dietary fibre (g/100 g)	12.35 ± 0.90^{a}	7.06 ± 0.52^{b}	5.63 ± 0.51^{c}	2.65 ± 0.81^{d}

aggregation, and the precipitation reaction was continued for 24 h at 4℃, followed by centrifugation under the same conditions.

Ultrasound-assisted Extraction

Ultrasound-assisted extraction (UAE) was carried out using an ultrasonic bath (Fisher Scientific, United Kingdom) operating at 40 kHz and 150 W for 20 min at pH 9.0, following Yang et al. (2024) with minor modifications. SLP was dispersed in deionised water at a solid–liquid ratio of 1:20 (w/v), and the pH of the suspension was adjusted to 9.0 using 0.1 M NaOH. It was then transferred into identical 250 mL cylindrical glass vessels and secured vertically at the centre of the ultrasonic bath using a clamp stand to prevent flotation and ensure a constant immersion depth throughout sonication. Continuous magnetic stirring (300 rpm) was applied during sonication to ensure uniform cavitation exposure. Samples (100 mL) were placed in identical 250-mL cylindrical glass vessels. Each vessel was supported using a clamp and positioned at the center of the water bath, where the external water level was maintained at a constant height of 6 cm to ensure consistent coupling and minimize variability associated with vessel geometry or distance from the transducers. The temperature of the extraction medium was maintained at 40 ± 2℃ by periodic addition of ice to the bath to prevent excessive thermal denaturation of proteins. After ultrasound treatment, the suspension was maintained at 40 ± 2℃ for 210 min and then centrifuged at 10,000 × g for 20 min at 4℃. The supernatant was subjected to isoelectric precipitation by adjusting the pH to 4.5 using 0.1 M HCl and the precipitation reaction was continued for 24 h at 4℃, followed by centrifugation.

Ultrafiltration-assisted Concentration

Ultrafiltration-assisted concentration (UF) was selected as a non-chemical, membrane-based concentration step to preserve protein structure while removing low-molecular-weight solutes. The process was carried out according to Anuar and Zuo (2025) with slight modifications. Briefly, UF was performed at a constant transmembrane pressure of 2.0 bar using nitrogen gas, with continuous stirring at 300 rpm to minimise concentration polarisation. The clarified alkaline extract was processed in a stirred ultrafiltration cell (Amicon® stirred cell, Millipore, Sigma-Aldrich, Gillingham, UK) fitted with a regenerated cellulose membrane with a molecular weight cut-off (MWCO) of 10 kDa and an effective membrane area of 28.7 cm^2. Filtration was continued until a volume reduction factor of approximately 3 was achieved, corresponding to a processing time of 45–60 min. These operating conditions were selected to balance protein retention with flux stability while minimising shear-induced protein denaturation. The resulting retentate was subsequently diafiltered with three volumes of deionised water under identical operating conditions to reduce residual salts and low-molecular-weight compounds.

All precipitated proteins were neutralised to pH 7.0 using 0.1 M NaOH and freeze-dried (FT33 MK11 vacuum freeze dryer, Armfield, United Kingdom) at −50℃ and 0.1 mbar for 48 h to obtain AE-IP_SPC, UAE_SPC, and UF_SPC protein concentrates. The dried protein concentrates were stored at −20℃ in airtight bags until further analysis.

For all functional and physicochemical measurements (protein solubility, foaming properties, and zeta potential), protein concentrates were dispersed in deionized water at the desired concentration and pH unless otherwise stated. This approach ensured that the measured properties reflected the intrinsic behavior of the proteins without interference from residual salts or other low-molecular-weight ions.

Physicochemical Characteristics of S. scabrum

Proximate Composition and Protein Yield

SLP and SPC were analysed for moisture, ash, fat, protein, starch, and dietary fibre. Moisture and fat were determined according to the AOAC 2008.06 official method (Leffler et al., 2008) using a CEM Smart 6 moisture analyser (CEM Corp., Matthews, NC, USA) and Oracle fat analyser (CEM

Corp., Matthews, NC, USA). Total ash was determined as the residue obtained after incinerating 2 g of each sample at 550 °C for 24 h. Total nitrogen content was determined by the Dumas combustion method using a LECO protein analyser (model FP828, LECO Instruments Ltd., Cheshire, United Kingdom), in accordance with AOAC Official Method 992.15. Briefly, freeze-dried powdered samples were dried in an oven (Gallenkamp, Cambridge, United Kingdom) to constant weight. Approximately 0.212 g of each sample was weighed into tin capsules and combusted at 950℃ in an oxygen-rich atmosphere. Nitrogen was quantified using a thermal conductivity detector, and the protein content was obtained using a nitrogen-to-protein conversion factor of 6.25. Dietary fibre content was determined using a Total Dietary Fibre Kit, following the enzymatic–gravimetric AOAC Method 991.43. Both soluble dietary fibre (SDF) and insoluble dietary fibre (IDF) fractions were determined, and total dietary fibre (TDF) was expressed as the sum of SDF and IDF. Starch content was determined using a Total Starch Assay Kit. Glucose release was quantified spectrophotometrically at 510 nm using the glucose oxidase/peroxidase (GOPOD) reagent, and total starch was expressed as a percentage of dry matter.

Protein extraction yield (%) was calculated as the mass of dried protein concentrate recovered after extraction relative to the initial dry weight of African nightshade leaves, according to Eq. 1, as the percentage of protein recovered relative to the total protein in the initial leaf powder (Kavle et al., 2023).

$$\text{Protein extraction yield (\%, w/w dry basis)} = \frac{(\text{Mconc, dry x Wprot, conc})}{(\text{Mleaf, dry})} \text{x}100 \quad (1)$$

where Mconc,dry is the dry mass of the protein concentrate (g), Wprot,conc is its protein mass fraction (g/g), and Mleaf,dry is the initial dry mass of leaf material (g).

Amino Acid Composition

The amino acid composition of the protein concentrate was determined according to Rezvankhah et al. (2021) using high-performance liquid chromatography (HPLC). Samples were hydrolysed in sealed glass tubes under a nitrogen atmosphere for 3 min using 6 M HCl (8 mL) at 120℃ for 22 h. After hydrolysis, the samples were transferred to 25 mL volumetric flasks and neutralized with 10 M NaOH (4.8 mL). The hydrolysates were filtered, and 1 mL of the filtrate was centrifuged at 1,000 × g for 10 min. An aliquot (400 µL) of the supernatant was analysed using an Agilent 1100 HPLC system (Agilent Technologies, Waldbronn, Germany) equipped with an autosampler and fluorescence detector. Separation was achieved on an ACE 3 µm C18 column (150 mm × 4.6 mm) maintained at 40℃. Amino acids were identified by comparison of retention times with those of 17 authenticated amino acid standards and quantified based on peak area using external calibration curves constructed from the corresponding standards. Amino acid contents were expressed as g per 100 g protein.

Colour

Colour of SPC was measured using a Minolta Chroma Meter (Model CR-400, Konica Minolta Sensing Inc., Osaka, Japan), previously calibrated with a standard white plate. Colour coordinates were recorded in the CIE L*ab** system, where L* represents lightness (0 = black, 100 = white), a* represents the green–red chromatic axis (negative = green, positive = red), and b* represents the blue-yellow axis (negative = blue, positive = yellow). To assess colour saturation and tone, chroma (C*) and hue angle (h°) values were calculated from a* and b* coordinates (Eq. 2 and Eq. 3). Using Eq. 4, ΔE values were computed using the CIELab coordinates of a previously characterised nettle leaf powder sample reported by Tanyitiku and Njombissie Petcheu (2025), which served as the reference for assessing overall colour deviation. The browning index (BI) was obtained according to Kavle et al. (2023) to assess the extent of browning induced during processing (Eq. 5).

$$\text{Chroma } (C^*) = \sqrt{a^{*2} + b^{*2}} \quad (2)$$

$$\text{Hue angle } (h^\circ) = arctan(b^*/a^*) \quad (3)$$

$$\Delta E^* = \sqrt{(L^* - L_0^*)^2 + (a^* - a_0^*)^2 + (b^* - b_0^*)^2} \quad (4)$$

$$\text{BI } (\%) = \frac{100\text{x } (\text{X} - 0.31)}{0.172} \quad (5)$$

$$\text{where X} = \frac{\text{a*+1.75L*}}{\text{5.645L*+ a -3.012b*}}$$

Techno-functional Properties

Protein Solubility

Protein solubility was determined as described by Kavle et al. (2023). Each sample was prepared at 1% (w/v) in deionised water, and the pH was adjusted to between 2 and 10 using 0.1 M HCl or 0.1 M NaOH. The suspensions were incubated at 40℃ for 1 h with gentle continuous shaking at

150 rpm and then centrifuged at 3,000 × g for 20 min. The protein content of the supernatant was quantified by total nitrogen (AOAC method 954.01) based on the Dumas principle using a nitrogen-to-protein conversion factor of 6.25. Protein solubility was calculated as the ratio of protein in the supernatant to the total protein content of the sample.

Water and Oil Holding Capacities

The water-holding capacity (WHC) and oil-holding capacity (OHC) of the protein concentrate were determined as described by Kavle et al. (2023), with slight modifications. Freeze-dried SPC (0.25 g) was mixed with 5 mL of deionized water (for WHC) or 5 mL of rapeseed oil (for OHC) at room temperature (25 ± 2℃) for 30 min on a gentle rotary shaker to ensure complete hydration or oil absorption. The mixtures were then centrifuged at 3,000 × g for 10 min. After centrifugation, the supernatant was carefully decanted and its volume measured. The volume of water or oil absorbed was calculated as the difference between the total volume added and the volume of supernatant recovered (that is, Vabsorbed = Vadded – Vsupernatant). WHC or OHC was then expressed as g per g protein by converting the absorbed volume to mass using the density of water (1.00 g/mL) or rapeseed oil (0.91 g/mL) as shown in Eq. 6.

$$\text{WHC or OHC (g/g)} = \frac{(\text{Vadded} - \text{Vsupernatant}) \text{ x density of liquid (g/mL)}}{\text{Msample (g)}} \quad (6)$$

where: Vadded = total volume of water or oil added (mL), Vsupernatant = volume of supernatant recovered after centrifugation (mL), density of liquid = density of the liquid (g/mL), water = 1.00 g/mL; rapeseed oil = 0.91 g/mL at 25 ± 2℃, Msample = initial sample mass (g).

Emulsifying Properties

Emulsifying activity index (EAI) and emulsion stability index (ESI) were determined according to Rezvankhah et al. (2021) with slight modifications. SPC samples (0.5% w/v) were homogenized with rapeseed oil at an oil:water ratio of 1:3 using a Thermomix TM6 (Vorwerk, Wuppertal, Germany) at 10,000 rpm for 2 min at 25℃. Immediately after homogenization, an aliquot of the emulsion was diluted 1:100 in 0.1% sodium dodecyl sulfate (SDS) solution and the absorbance at 500 nm was measured (A_0) with 0.1% SDS serving as the control. After 10 min, another aliquot was sampled for absorbance measurement (A_{10}). EAI (m^2/g) and ESI (min) were calculated using Eq. 7 and Eq. 8, respectively.

$$\text{EA } (\frac{\text{m2}}{\text{g}}) = \frac{2 \times 2.303 \times \text{Ao} \times D}{C \times \varnothing \times L \times 10000} \quad (7)$$

$$\text{ESI (min)} = \frac{Ao}{A0 - A10} \text{x10} \quad (8)$$

where C is the protein concentration (g/mL), D is the dilution factor, ϕ is the oil volume fraction (specifically set at 0.25), and L is the path length of cuvette (cm).

Foaming Properties

Foaming properties were measured using the standard aeration-volume displacement method at pH 7.0 (Kavle et al., 2023). SPC dispersions (1% w/v) in deionised water were whipped in a graduated cylinder using a hand-held homogeniser (12,000 rpm, 2 min). Foaming capacity (FC) was calculated using Eq. 9 and foaming stability (FS) was recorded as the percentage of foam volume retained after 30 min.

$$\text{FC (\%)} = \frac{Vo - Vb}{Vb} \text{x100} \quad (9)$$

where V_0 is the foam volume immediately after whipping and Vb is the initial liquid volume.

Protein Coagulation

The heat-induced coagulation of SPC was determined as described by Mishyna et al. (2019). SPC samples (1% w/v) were prepared in 10 mL of phosphate buffer (pH 7.0) and gently stirred with a magnetic stir bar for 5 min. It was then centrifuged (Heraeus Megafuge 8 centrifuge, Thermo Scientific, United Kingdom) at 3,500 × g for 15 min at 25℃. To prepare the 'before heating' samples, 8 mL of Biuret reagent was added to 2 mL of the suspension and incubated in the dark for 30 min. Absorbance was then measured at 540 nm using a UV–Vis spectrophotometer (Jenway, Cole-Parmer, United Kingdom). The 'after heating' sample was prepared by heating the remaining supernatant for 15 min in a 100℃-water bath (Thermo Scientific Precision water bath, United Kingdom) before measuring the absorbance at 540 nm. The heat-induced coagulation was calculated using Eq. 10.

$$\text{Heat} - \text{induced coagulation (\%)} = \frac{\text{Abef} - \text{Aaft}}{\text{Abef}} \text{x100} \quad (10)$$

where Abef, absorbance of before heating, and Aaft, absorbance after heating.

Calcium-induced coagulation was carried out as described by Lu et al. (2010) with slight modification. SPC dispersions (5% w/v) were prepared at pH 7.0 as described above. A 1 M calcium chloride ($CaCl_2$) solution was prepared in deionised water and added to the dispersions to achieve a final concentration of 10 mM. The mixtures were gently stirred for 10 min and then incubated at 25 ± 2℃ for 8 h to allow protein-calcium interactions. This was then centrifuged at 10,000 × g for 15 min at 20℃. The protein content in the supernatant was quantified, and the percentage of coagulated protein was calculated using Eq. 11.

$$\text{Calcium} - \text{induced coagulation}\ (\%) = \frac{A0 - Ac}{A0} \text{x}100 \quad (11)$$

where A0 absorbance of protein dispersion before $CaCl_2$ addition, and Ac absorbance of supernatant after $CaCl_2$-induced coagulation.

Water release from heat-induced protein gels was determined to assess gel network stability. After heat treatment and cooling, coagulated samples were centrifuged at 3,000 × g for 10 min at 20℃. The mass of released water was recorded, and water release was expressed as a percentage of the initial sample mass.

Coagulation temperature was determined following the coagulation test procedure described by Uddin et al. (2000), with minor modifications. SPC samples (1% w/v) were prepared in phosphate buffer (pH 7.0), and 10 mL of the suspension was transferred into a test tube and placed in a thermostatically controlled shaker water bath. The suspension was heated at a controlled rate such that the temperature difference between the water bath and the sample did not exceed 1–1.5℃, while being gently agitated to ensure uniform heating. Coagulation temperature was defined as the temperature at which the first visible signs of protein aggregation or curd formation were observed, as determined by visual inspection under continuous stirring using a calibrated temperature probe.

Bulk and Tapped Densities

Bulk and tapped densities of SPC was determined according to Etti (2020). The powder was gently added to a 50 mL measuring cylinder until it reached the 50 mL mark. For the bulk density, the cylinder was dropped from a height of 1 inch onto a wooden surface at 2-s intervals, and the final volume was recorded. Tap density was determined by tapping the cylinder 500 times and the volume was recorded once it stabilised, reflecting the powder's compactness after tapping.

Carr index, Hausner Ratio

The Carr index (CI) and Hausner ratio (HR) were obtained as described by Mochahary et al. (2022). CI was determined by calculating the percentage difference between the tapped density and bulk density, divided by the tapped density. HR was calculated as the ratio of tapped density to bulk density. According to Carr's flowability classification, a CI value between 5 and 15% indicates excellent flowability, and > 25% suggest poor flowability, HR values between 1.0 and 1.1 indicate excellent flowability, 1.1 to 1.25 indicate moderate flow, between 1.25 and 1.4 suggests poor flow, and > 1.4 indicate extremely low flowability (Awari et al., 2025).

Angle of Repose

The angle of repose (θ) was determined as described by Awari et al. (2025). Each SPC powder was placed into a funnel positioned 6 cm above a level surface and allowed to freely flow, forming a conical heap on a horizontally placed sheet of paper. The height (h) of the conical heap and the radius (r) of its base were measured, and the angle of repose was calculated using the relationship in Eq. 12. Angles near 30° indicate good flowability, while values approaching 40° suggest poor flow.

Equation 12 $\theta = \tan^{-1}(h/r)$.

Structure of S. scabrum Leaf Protein

Zeta Potential and Particle Size Analysis

Zeta potential (ζ-potential) and particle size distribution of SPC (1 mg/mL) dissolved in deionised water were measured using a HORIBA SZ-100Z Nanoparticle Analyzer (HORIBA Ltd, Kyoto, Japan). Zeta potential was determined at pH between 2 and 10 by electrophoretic light scattering, while particle size was measured using Dynamic Light Scattering (DLS) mode. Results were reported as mean zeta potential, Z-average hydrodynamic diameter and Polydispersity Index (PDI). Due to protein aggregation, values represent aggregate size rather than primary particles. Notably, dispersions with absolute ζ-potential of ≥ 30 mV tend to be very stable, whereas those with lower absolute zeta values (≤ 20 mV) are prone to flocculation or settling over time (Acar et al., 2025).

Scanning Electron Microscopy

The morphological features of SLP and SPC were examined using a ZEISS Sigma Field Emission Scanning Electron Microscope (ZEISS GeminiSEM500, Oberkochen, Germany). Approximately 2–3 mg of powdered sample was mounted on aluminium stubs using double-sided carbon tape and sputter-coated with a 5 nm layer of gold–palladium prior to imaging. Scanning electron micrographs were obtained at an accelerating voltage of 5 kV and magnifications of

3,000×, 6,000×, and 10,000× to evaluate powder morphology, porosity, and structural integrity.

Fourier Transform Infrared Spectroscopy

FTIR was used as a comparative, qualitative tool to assess relative conformational changes among AE-IP_SPC, UAE_SPC, and UF_SPC protein concentrates. Secondary structural features of SPC were analysed using an FTIR spectrometer (PerkinElmer Spectrum Two, L1600235, Beaconsfield, United Kingdom) and processed using Spectrum IR 10.6.2 software. (FTIR spectra were recorded over the wavenumber range of 4,000–400 cm^{-1} using 32 scans at a resolution of 4 cm^{-1}). Spectral interpretation followed established literature, where the amide I region (1600–1700 cm^{-1}) is primarily associated with C = O stretching vibrations and is sensitive to protein secondary structure, with α-helix typically assigned to 1650–1658 cm^{-1} and β-sheet structures to 1638–1687 cm^{-1} (Kavle et al., 2023). Amide II bands arise mainly from N–H bending coupled with C-N stretching vibrations, while amide III bands reflect contributions from α-helix (1290–1340 cm^{-1}), β-sheet (1181–1248 cm^{-1}), and random coil structures (1255–1288 cm^{-1}) (Kavle et al., 2023). In this study, quantitative secondary structure determination based on amide I band deconvolution was not performed due to significant band overlap and the heterogeneous composition of the leaf protein concentrates.

Statistical Analysis

All measurements were carried out in triplicate. Results were expressed as mean ± standard deviation. Data were analysed using one-way ANOVA followed by Tukey's test at $p < 0.05$ using IBM SPSS v.31.0.0.0 (117) (IBM Corp., Armonk, NY, USA).

Results and Discussion

Proximate Composition and Protein Yield

The proximate composition of SLP is presented in Table 1. SLP exhibited high protein (31.54 g/100 g), ash (13.76 g/100 g), and total dietary fiber (12.35 g/100 g), indicating the nutritional richness of the raw material. These values are consistent with previous reports on African nightshade leaves, where similarly high ash (13.91- 17.18 g/100 g) and dietary fibre (28,67- 35.78 g/100 g), along with protein levels ranging from 31 to 38 g/100 g, have been reported (Bayang et al., 2025; Lugumira et al., 2025; Njong et al., 2023). Compared with other leafy materials, the protein content of SLP in this study exceeded that of alfalfa (26%) (Hojilla-Evangelista et al., 2017), spinach (8.37–8.75%) (Bando et al., 2025), blackberry (24.34%), and moringa (6.72%) (Bocarando-Guzmán et al., 2022), thus, highlighting its suitability as a protein source.

Furthermore, the moisture, fat, and total fiber contents were consistently low across all SPC protein concentrates at 5.53–6.91 g/100 g, 1.12–2.03 g/100 g, and 2.65–7.06 g/100 g, respectively, indicating effective removal of non-protein components. The highest fiber residue (7.06 ± 0.52 g/100 g) observed in AE-IP_SPC may be associated with the persistence of protein-cell wall associations during extraction. Similarly, ash content was significantly ($p < 0.05$) higher in AE-IP_SPC (7.63 ± 0.81 g/100 g) and UAE_SPC (6.62 ± 0.18 g/100 g) than in UF_SPC (4.53 ± 0.22 g/100 g), reflecting salt incorporation during alkaline extraction and pH adjustment steps. In UF_SPC, the reduced ash content may be attributed to the removal of soluble minerals during membrane filtration and diafiltration, as has been reported for other plant protein concentrates (Anuar & Zuo, 2025; Hojilla-Evangelista et al., 2017; Illingworth et al., 2024).

Protein yield differed significantly ($p < 0.05$) among processing methods (Table 1). UAE_SPC exhibited the highest protein yield (48.71%), followed by AE-IP_SPC (34.02%) and UF_SPC (26.45%), corresponding to approximately 48.7 g, 34.0 g, and 26.5 g of protein concentrate obtained from 100 g of dry leaf powder, respectively. Mishyna et al. (2019) reported similar protein yields of 39.6% and 55.2% for *A. mellifera* following alkaline and ultrasound-assisted extractions, respectively, with an additional sonication step increasing the yield by a further 6.4% compared with alkaline extraction alone (3.3%). The enhanced recovery achieved by UAE is attributed to cavitation-induced cell wall disruption and improved mass transfer, which facilitate protein release and solubilization (Cheng et al., 2021; Ragazzo-Calderón et al., 2024). Although UF_SPC showed lower recovery, it exhibited a relatively high protein purity (71.43 g/100 g), reflecting the effectiveness of membrane separation in concentrating macromolecular proteins under mild conditions, without exposure to extreme pH or thermal stress (Illingworth et al., 2024; Pakawan, 2022). These results demonstrate that AE-IP, UAE, and UF significantly influence the yield and compositional quality of *S. scabrum* protein concentrates, whereby UAE maximised protein recovery, while UF provided a milder processing route that favoured higher protein purity.

Results are expressed as mean ± standard deviation (n = 3) and means with different superscripts in the same row are significantly ($p < 0.05$) different. SLP: *S. scabrum* leaf powder; AE-IP_SPC: alkaline extraction-isoelectric

precipitation, UAE_SPC: ultrasound-assisted extraction, and UF_SPC: ultrafiltration.

Amino Acid Composition

The essential and non-essential amino acid compositions of *S. scabrum* protein concentrates are presented in Table 2. Glutamic acid (13.4–14.3 g/100 g protein) and aspartic acid (9.2–9.7 g/100 g protein) were the predominant amino acids, consistent with profiles reported for other green leafy proteins such as cauliflower by-products (Xu et al., 2017a, 2017b), moringa (Bocarando-Guzmán et al., 2022), alfalfa (Hojilla-Evangelista et al., 2017; Pérez-Vila et al., 2022) and perennial ryegrass (Pérez-Vila et al., 2024). Among the essential amino acids, leucine, valine, lysine, and phenylalanine were present at appreciable levels, underscoring the nutritional relevance of *S. scabrum* protein (Lugumira et al., 2025). The relatively high lysine content (5.4–5.9 g/100 g protein) is particularly noteworthy, as lysine is frequently limited in cereal-based diets (FAO/WHO/UNU, 2007; Pakawan, 2022).

Only minor variations in individual amino acid contents were observed among AE-IP_SPC, UAE_SPC, and UF_SPC, although some significant differences ($p < 0.05$) were detected (Table 2). When expressed relative to product composition, UF_SPC provided the highest amount of essential (38.4 g/100 g protein) and non-essential (48.5 g/100 g protein) amino acids per unit mass, likely due to its higher overall protein content (Table 1). The higher total amino acid contents compared to crude protein values in this study could have arisen from methodological differences, as crude protein was estimated from total nitrogen using a fixed conversion factor, whereas amino acid analysis quantified the actual mass of amino acids following hydrolysis. Similar discrepancies between crude protein and total amino acids have been widely reported for leaf-derived and plant-based protein systems (Ma et al., 2022; Pérez-Vila et al., 2022, 2024).

In addition, UF_SPC exhibited the most consistent amino-acid profile, with slightly greater retention of sensitive amino acids such as methionine (1.9 g/100 g) and cysteine (1.0 g/100 g). In contrast, AE-IP_SPC showed lower levels of these sulphur-containing amino acids, methionine (0.9 g/100 g) and cysteine (0.4 g/100 g), likely due to their susceptibility to alkaline-induced degradation and oxidative reactions during pH shifting and isoelectric precipitation. Similar reductions in sulphur amino acids have been reported in alkaline-extracted leaf and legume proteins (Acar et al., 2025; Bocarando-Guzmán et al., 2022; Maag et al., 2025).

Table 2 Amino acid profile (g/100 g protein) of *S. scabrum* leaf, alfalfa leaf and soy proteins

Amino acid	AE-IP_SPC	UAE_SPC	UF_SPC	Alfalfa (Hojilla-Evangelista et al., 2017)	Soy (Ma et al., 2022)	FAO/WHO adult requirement (WHO/FAO/UNU, 2007)
Essential						
Histidine (His)	2.2 ± 0.02^{c}	2.3 ± 0.00^{b}	2.4 ± 0.04^{a}	2.37	2.22 ± 0.01	1.5
Isoleucine (Ile)	3.9 ± 0.01^{c}	4.0 ± 0.05^{b}	4.2 ± 0.02^{a}	5.50	4.35 ± 0.03	3.0
Leucine (Leu)	6.8 ± 0.00^{b}	6.9 ± 0.02^{a}	7.2 ± 0.07^{a}	9.08	6.95 ± 0.02	5.9
Lysine (Lys)	5.4 ± 0.04^{c}	5.5 ± 0.02^{b}	5.9 ± 0.00^{a}	6.00	5.45 ± 0.02	4.5
Methionine (Met)	0.9 ± 0.00^{c}	1.8 ± 0.04^{b}	1.9 ± 0.08^{c}	1.75	1.00 ± 0.03	1.6
Phenylalanine (Phe)	4.5 ± 0.02^{c}	4.7 ± 0.02^{b}	4.8 ± 0.05^{a}	5.79	4.62 ± 0.01	-
Threonine (Thr)	3.6 ± 0.05^{c}	3.7 ± 0.01^{b}	3.8 ± 0.02^{a}	5.13	3.24 ± 0.03	2.3
Valine (Val)	4.3 ± 0.01^{c}	4.7 ± 0.00^{b}	4.9 ± 0.02^{a}	6.62	7.17 ± 0.26	3.9
Total	36.5 ± 0.04^{c}	37.9 ± 0.04^{b}	38.4 ± 0.08^{a}	43.44	-	-
Non-essential						
Alanine (Ala)	4.0 ± 0.08^{c}	4.1 ± 0.00^{b}	4.3 ± 0.02^{a}	5.97	3.73 ± 0.01	-
Arginine (Arg)	4.8 ± 0.00^{c}	5.0 ± 0.01^{b}	5.2 ± 0.08^{a}	5.53	6.52 ± 0.01	-
Aspartic acid (Asp)	9.2 ± 0.04^{c}	9.5 ± 0.05^{b}	9.7 ± 0.00^{a}	10.84	9.61 ± 0.05	-
Cysteine (Cys)	0.4 ± 0.04^{c}	0.9 ± 0.03^{b}	1.0 ± 0.02^{a}	1.50	0.85 ± 0.01	-
Glutamic acid (Glu)	13.4 ± 0.02^{c}	13.7 ± 0.08^{b}	14.3 ± 0.00^{a}	12.37	13.27 ± 0.28	-
Glycine (Gly)	4.1 ± 0.01^{c}	4.2 ± 0.02^{b}	4.3 ± 0.03^{a}	6.01	3.63 ± 0.01	-
Proline (Pro)	4.3 ± 0.07^{c}	4.4 ± 0.08^{b}	4.5 ± 0.06^{a}	5.27	4.60 ± 0.01	-
Serine (Ser)	3.8 ± 0.02^{c}	4.2 ± 0.01^{b}	4.4 ± 0.05^{a}	4.50	4.26 ± 0.12	-
Tyrosine (Tyr)	3.2 ± 0.08^{c}	3.6 ± 0.07^{b}	3.9 ± 0.08^{a}	4.56	2.83 ± 0.01	-
Total	45.2 ± 0.06^{c}	46.3 ± 0.02^{b}	48.5 ± 0.04^{a}	-	-	-

Comparison with FAO/WHO reference patterns for adult protein requirements showed that all protein concentrates met or exceeded recommended levels for most essential amino acids (Table 2). For instance, leucine and lysine levels exceeded FAO/WHO recommendations, with lysine being particularly relevant for complementing cereal-based diets where it is often limiting (Njong et al., 2023; Pakawan, 2022). For contextual evaluation, the amino acid profile of *S. scabrum* protein was also compared with soybean protein, a widely accepted benchmark for plant protein quality, and alfalfa leaf protein, a representative leaf-derived protein source with similar structural and extraction characteristics. Here, sulfur-containing amino acids were the primary limiting factors, with concentrations comparable to alfalfa (Hojilla-Evangelista et al., 2017) and higher than soy (Ma et al., 2022) (Table 2).

Results are expressed as mean ± standard deviation (n = 3) and means with different superscripts in the same row are significantly ($p < 0.05$) different. AE-IP_SPC: alkaline extraction-isoelectric precipitation, UAE_SPC: ultrasound-assisted extraction, and UF_SPC: ultrafiltration.

Color Characteristics

Significant colour differences ($p < 0.05$) were observed among AE-IP_SPC, UAE_SPC, and UF_SPC (Table 3). AE-IP_SPC exhibited significantly lower lightness (L* = 57.89 ± 0.17) and higher browning index (BI = 42.90 ± 0.54) compared with UAE_SPC (L* = 63.76 ± 0.40; BI = 28.56 ± 0.08) and UF_SPC (L* = 71.53 ± 0.22; BI = 20.76 ± 0.11), indicating a darker appearance and greater browning following alkaline extraction-isoelectric precipitation. The pronounced browning in AE-IP_SPC can be attributed to prolonged exposure to alkaline conditions and subsequent acid precipitation, which promote chlorophyll degradation, pheophytin formation, and non-enzymatic browning reactions involving phenolics and proteins (Awari et al., 2025). Similar darkening effects following alkaline extraction have been reported for moringa and other leafy protein isolates (Bocarando-Guzmán et al., 2022) as well as sago palm weevil proteins (Kavle et al., 2023).

Table 3 Color characteristics of *S. scabrum* protein concentrates

Parameters	AE-IP_SPC	UAE_SPC	UF_SPC
L*	57.89 ± 0.17^{c}	63.76 ± 0.40^{b}	71.53 ± 0.22^{a}
a*	−1.54 ± 0.04^{a}	−2.69 ± 0.33^{b}	−2.90 ± 0.56^{b}
b*	21.49 ± 0.27^{a}	17.89 ± 0.31^{b}	14.92 ± 0.08^{c}
ΔE	24.31 ± 0.52^{c}	28.55 ± 0.61^{b}	35.53 ± 0.92^{a}
Chroma (C*)	20.43 ± 0.63^{a}	18.53 ± 0.60^{b}	13.62 ± 0.61^{c}
Hue angle (h^{o})	95.32 ± 0.81^{b}	98.45 ± 0.62^{b}	102.57 ± 0.48^{a}
Browning Index (%)	42.90 ± 0.54^{a}	28.56 ± 0.08^{b}	20.76 ± 0.11^{c}

Changes in chromatic coordinates further reflected extraction-induced modifications. AE-IP_SPC showed higher b* (21.49) and a less negative a* (−1.54), indicating a shift toward a more yellowish tone. Similar trends have been reported for moringa protein isolates, which showed lower L* and b* values and appeared darker than soy protein isolates after alkaline extraction (Bocarando-Guzmán et al., 2022). In contrast, UF_SPC exhibited lower b* (14.92) and a more negative a* (−2.90), reflecting a duller but greener appearance. Hue angle and chroma supported these observations: AE-IP_SPC displayed lower hue angle (95.32°) and higher chroma (20.43), indicating more saturated coloration, whereas UF_SPC showed the lowest chroma (13.62), suggesting reduced colour intensity.

The overall colour difference (ΔE) relative to the original leaf powder increased in the order AE-IP_SPC (24.64) < UAE_SPC (28.55) < UF_SPC (35.52). The larger ΔE observed for UF_SPC was primarily driven by increased lightness rather than browning, reflecting pigment removal and structural clarification rather than thermal or chemical degradation.

UAE_SPC exhibited intermediate colour characteristics, with a substantially higher lightness (L* = 63.76) and a large overall colour difference (ΔE = 28.55) relative to the previously reported original nettle leaf powder (L* = 36.52 ± 1.13, a* = −6.88 ± 0.97, b* = 10.44 ± 0.90; Tanyitiku & Njombissie Petcheu, 2025). Ultrasound treatment may accelerate pigment degradation through localized heating and radical formation (Khan et al., 2024); however, shorter extraction times and controlled temperatures likely limited excessive browning, resulting in color attributes superior to AE-IP_SPC.

For UF_SPC, the highest lightness (L* = 71.53) and the lowest browning index (BI = 20.76) indicate a markedly lighter appearance with minimal browning. The overall colour difference relative to the original nettle leaf powder was also the greatest (ΔE = 35.53), signifying a substantial deviation from the native leaf colour (Tanyitiku & Njombissie Petcheu, 2025). This colour preservation in terms of reduced browning, despite the large ΔE driven largely by increased lightness, is attributable to the mild, non-denaturing nature of membrane-based processing and the absence of extreme pH shifts, which together limit pigment degradation and Maillard-type browning reactions (Pakawan, 2022). Comparable trends have been reported for ultrafiltered leafy protein concentrates (Furia et al., 2025; Maag et al., 2025; Pakawan, 2022).

From an application perspective, lighter protein powders with low browning are advantageous for incorporation into beverages, dairy analogues, and protein-fortified products where colour neutrality is desirable (Ismail et al., 2020; Qin

et al., 2022). Overall, colour quality was strongly dependent on extraction severity, with ultrafiltration best preserving visual attributes, whereas alkaline extraction promoted browning and pigment transformation.

Results are expressed as mean ± standard deviation (n = 3) and means with different superscripts in the same row are significantly ($p < 0.05$) different. AE-IP_SPC: alkaline extraction-isoelectric precipitation, UAE_SPC: ultrasound-assisted extraction, and UF_SPC: ultrafiltration.

Techno-functional Properties

Protein Solubility as a Function of pH

The solubility profiles of *S. scabrum* leaf protein are presented in Fig. 1. At pH 2, UF_SPC showed significantly ($p < 0.05$) higher solubility (78.24 ± 0.33%) than UAE_SPC (61.04 ± 1.72%) and AE-IP_SPC (58.44 ± 0.97%). Solubility declined sharply at pH 4 for all samples, after which it rose progressively at pH 6. At pH 8–10, a consistent rank order emerged, UF_SPC > UAE_SPC > AE-IP_SPC, with UF_SPC significantly ($p < 0.05$) achieving the highest solubility (92.41 ± 0.22%) and AE-IP_SPC the lowest (72.37 ± 0.08%). The comparatively lower solubility of AE-IP_SPC across the curve, most evident at pH 8–10, likely reflects structural alteration and aggregation introduced during alkaline treatment (Cruz-Solis et al., 2023; Yao et al., 2023). Accordingly, a recent study on yellow pea proteins (Anuar & Zuo, 2025) reported that ultrafiltration, often combined with diafiltration, can achieve high protein recovery while preserving higher native solubility compared with AE-IP. UF is a membrane-based, low-shear, non-precipitative route that concentrates proteins while removing small solutes (salts, phenolics, low-MW inhibitors) and minimising chemical/thermal stresses, helping to preserve native-like structure and interfacial behaviour (John et al., 2024). As such, its superior solubility may be attributed to the mild processing conditions employed, which limit protein denaturation and preserve native-like conformations (Huang et al., 2024; Muller et al., 2024).

In contrast, UAE_SPC consistently showed improved solubility relative to AE-IP_SPC at all pH values outside the isoelectric region. This improvement is consistent with the acoustic cavitation mechanism, where microstreaming and shear can reduce particle size, disrupt aggregates, and partially unfold proteins to expose hydrophilic sites, effects known to enhance hydration and solubility without extensive thermal loads (Ragazzo-Calderón et al., 2024; Zhang et al., 2024; Zheng et al., 2019). Moreover, UAE has been shown to increase extractability and functional properties (solubility, emulsification, foaming) of leaf proteins such as moringa (Cheng et al., 2021; Khan et al., 2024), jackfruit (Ragazzo-Calderón et al., 2024), mulberry (Zhao et al., 2023), duckweed (Maag et al., 2025) as well as soy protein isolates (Zheng et al., 2019).

Overall, the solubility patterns align with the characteristic U-shaped dependence on pH, showing a pronounced minimum around pH ~ 4 and marked increases as pH shifts away from the isoelectric region (pI), a behaviour widely reported for plant (Bocarando-Guzmán et al., 2022; Ladjal-Ettoumi et al., 2016; Maag et al., 2025; Qin et al., 2022) and insect proteins (Kavle et al., 2023). For applications requiring high solubility at neutral to alkaline pH (for example, high-protein beverages, batters, or emulsions), UF, and to a lesser extent UAE, should be favoured to

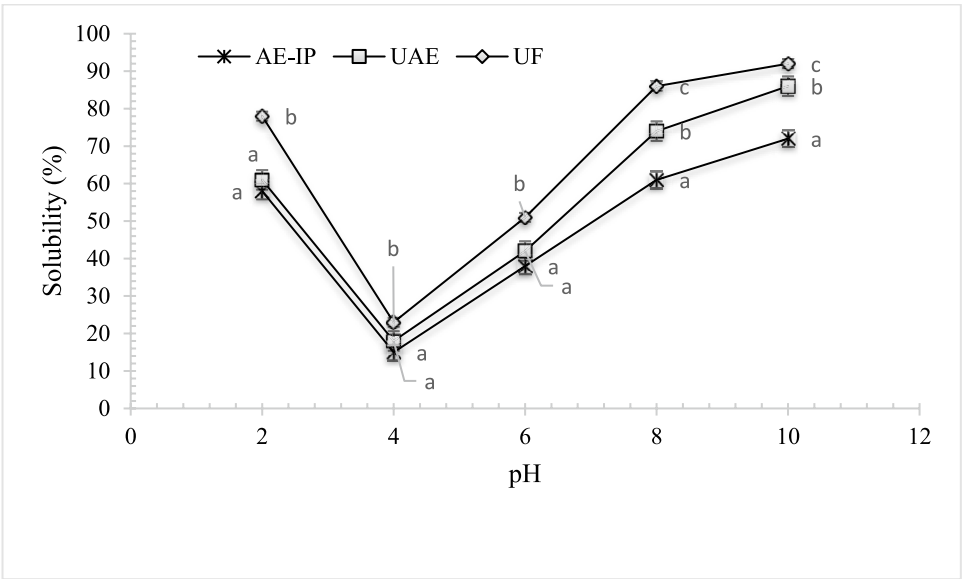

Fig. 1 Solubility trend of *Solanum scabrum* leaf protein

Table 4 Techno-functional properties of *S. scabrum* protein concentrates

Properties	AE-IP_SPC	UAE_SPC	UF_SPC
WHC (g water/g protein)	2.45 ± 0.04^{c}	3.5 ± 0.11^{a}	3.1 ± 0.20^{b}
OHC (g oil/g protein)	1.62 ± 0.05^{c}	2.36 ± 0.01^{b}	2.51 ± 0.04^{a}
FC (%)	48.92 ± 0.00^{c}	71.62 ± 0.04^{b}	78.63 ± 0.05^{a}
FS (%)	33.06 ± 0.02^{c}	56.29 ± 0.02^{b}	69.48 ± 0.00^{a}
EAI (m^2/g)	0.318 ± 0.01^{c}	0.385 ± 0.04^{a}	0.367 ± 0.04^{b}
ESI (min)	36.06 ± 0.08^{c}	42.34 ± 0.00^{b}	59.01 ± 0.55^{a}
Heat-induced coagulated protein (%)	74.35 ± 0.04^{a}	68.79 ± 0.01^{b}	61.34 ± 0.08^{c}
Calcium-induced coagulated protein (%)	11.15 ± 0.02^{a}	7.69 ± 0.01^{b}	4.63 ± 0.00^{c}
Coagulation temperature (℃)	73.7 ± 0.08^{c}	78.6 ± 0.02^{b}	85.9 ± 0.08^{a}
Water release after coagulation (%)	46.71 ± 0.00^{a}	27.40 ± 0.08^{b}	15.42 ± 0.01^{c}

retain functional performance, whereas AE-IP may require post-processing interventions (such as pH-shift resolubilisation) to achieve comparable solubility (Tables 4 and 5).

Water and Oil Holding Capacities

The water (WHC) and oil-holding capacity (OHC) differed significantly ($p < 0.05$) among AE-IP_SPC, UAE_SPC and UF_SPC (Table 3). UAE_SPC exhibited the highest WHC (3.5 g/g), followed by UF_SPC (3.1 g/g) and AE-IP_SPC (2.45 g/g). This could be attributed to ultrasound-induced structural loosening and particle size reduction, as confirmed by SEM (Fig. 3) and particle size distribution (Table 6), as smaller, more porous particles provide greater surface area and more accessible polar sites for hydrogen bonding with water molecules (Kavle et al., 2023; Maag et al., 2025). Similarly, the WHC results for UF_SPC may result from retention of hydrophilic functional groups and minimal aggregation during processing, preserving native-like conformations and water-binding sites, consistent with previous reports on ultrafiltered leaf proteins (Dirr & Karslioglu, 2024; Gasparre et al., 2025; John et al., 2024).

OHC is influenced by exposure of hydrophobic regions within the protein matrix. UF_SPC showed the highest OHC (2.51 g/g), followed by UAE_SPC (2.36 g/g) and AE-IP_SPC (1.62 g/g). The retention of higher-molecular-weight protein fractions during UF, combined with increased protein–protein interactions and mild shear and confinement within the membrane system, could have promoted conformational rearrangements that increased the availability of hydrophobic domains at the protein surface (Maag et al., 2025; Pakawan, 2022). In contrast to ultrasound-assisted extraction, where cavitation can directly unfold proteins, ultrafiltration influences protein surface properties primarily through fractionation and concentration effects. As such, the enhanced exposure of hydrophobic amino acid residues observed in UF_SPC is not attributed to cavitation or gas–liquid interface adsorption, but rather to selective fractionation and concentration effects during ultrafiltration. These findings suggest that both particle size reduction and controlled protein unfolding play key roles in determining hydration and lipid-binding properties.

Table 5 Flowability of *S. scabrum* protein concentrates

Parameters	AE-IP_SPC	UAE_SPC	UF_SPC
Tap density (g/cm^3)	0.48 ± 0.06^{c}	0.55 ± 0.08^{b}	0.59 ± 0.00^{a}
Bulk density (g/cm^3)	0.34 ± 0.01^{c}	0.43 ± 0.08^{b}	0.48 ± 0.00^{a}
Carr's index (%)	28.61 ± 0.08^{a}	20.41 ± 0.08^{b}	18.71 ± 0.02^{c}
Hausner's ratio	1.41 ± 0.04^{a}	1.28 ± 0.00^{b}	1.22 ± 0.02^{c}
Angle of repose (°)	34.60 ± 0.28^{a}	34.51 ± 0.33^{a}	30.67 ± 0.45^{b}

Emulsifying Properties

The emulsifying activity index (EAI) and emulsion stability index (ESI) of AE-IP_SPC, UAE_SPC, and UF_SPC differed significantly ($p < 0.05$). UF_SPC exhibited the highest ESI (59.01 min), followed by UAE_SPC (42.34 min) and AE-IP_SPC (36.06 min). The superior stability of UF_SPC is likely attributed to its higher solubility (Fig. 1), smaller particle size (Table 6), and greater absolute zeta potential (Fig. 2), which enhance electrostatic repulsion between oil droplets and reduce flocculation and coalescence. In contrast, UAE_SPC exhibited the highest EAI (0.385 m^2/g), followed by UF_SPC (0.367 m^2/g) and AE-IP_SPC (0.318 m^2/g). The enhanced emulsifying activity of UAE_SPC may be associated with reduced particle size and partial protein unfolding induced by ultrasound treatment, which improves interfacial adsorption and surface hydrophobicity,

Table 6 Particle size of *S. scabrum* protein concentrates

Parameters	AE-IP_SPC	UAE_SPC	UF_SPC
Particle size (nm)	$28{,}653.23 \pm 6.57^{a}$	$6{,}716.32 \pm 5.30^{b}$	$1{,}994.45 \pm 4.15^{c}$
PDI	0.53 ± 0.05^{a}	0.37 ± 0.21^{b}	0.22 ± 0.08^{c}

as previously reported for ultrasound-modified plant proteins (Cheng et al., 2021; Kadam et al., 2015; Khan et al., 2024). The comparatively lower EAI observed for AE-IP_SPC is likely due to extensive aggregation and reduced molecular flexibility resulting from alkaline extraction and isoelectric precipitation, which limit rapid adsorption and rearrangement at the oil–water interface (Dirr & Karslioglu, 2024; Illingworth et al., 2024; Xu et al., 2017a, 2017b).

Foaming Properties

Foaming capacity (FC) and foam stability (FS) of AE-IP_SPC, UAE_SPC, and UF_SPC are presented in Table 4. UF_SPC demonstrated the highest FC (78.63%) and FS (69.48%), followed by UAE_SPC (FC: 71.62%, FS: 56.29%) and AE-IP_SPC (FC: 48.92%, FS: 33.06%). The superior foaming performance of UF_SPC can be attributed to its higher solubility, smaller particle size, and greater absolute zeta potential, which facilitate rapid diffusion and adsorption at the air–water interface while promoting electrostatic repulsion between air bubbles, thereby enhancing foam stability. UAE_SPC exhibited intermediate foaming properties, likely due to partial protein unfolding and reduced particle size induced by ultrasound treatment, which improve interfacial adsorption and surface activity (Kadam et al., 2015; Khan et al., 2024). In contrast, AE-IP_SPC showed the lowest foaming performance, likely resulting from extensive aggregation and reduced molecular flexibility caused by alkaline extraction and isoelectric precipitation (Hojilla-Evangelista et al., 2017; Illingworth et al., 2024). Such aggregation limits rapid interfacial adsorption and weakens film formation. Overall, effective foaming requires a balance between structural flexibility and molecular integrity. Proteins must be sufficiently flexible to adsorb and unfold at the interface, yet structurally intact to form cohesive and elastic interfacial films that resist bubble coalescence (Maag et al., 2025; Muller et al., 2024; Pakawan, 2022).

Coagulation and Gelation Behavior

Heat- and calcium-induced coagulation of AE-IP_SPC, UAE_SPC, and UF_SPC differed ($p < 0.05$) significantly (Table 4), reflecting extraction-induced structural modifications. AE-IP_SPC exhibited the highest heat-induced coagulation (74.35%) and the lowest coagulation temperature (73.7℃), indicating reduced thermal stability. This behavior is attributed to extensive alkaline extraction and isoelectric precipitation, which promote partial unfolding and exposure of reactive sulfhydryl and hydrophobic groups, facilitating rapid aggregation during heating (Cruz-Solis et al., 2023; Yao et al., 2023). UAE_SPC exhibited intermediate behavior, consistent with partial structural disruption induced by ultrasonic cavitation without extensive chemical modification (Zhang et al., 2024). In contrast, UF_SPC showed the lowest heat-induced coagulation (61.34%) but the highest coagulation temperature (85.9℃), suggesting improved thermal stability due to preservation of more native and compact protein structures (Anuar & Zuo, 2025).

Calcium-induced coagulation further differentiated the concentrates. UF_SPC required significantly lower Ca^{2+} concentrations (4.63%) to induce coagulation compared with UAE_SPC (7.69%) and AE-IP_SPC (11.15%), indicating greater availability of negatively charged residues and enhanced ionic responsiveness. This observation aligns with its higher absolute zeta potential values at neutral pH (Fig. 2) and supports improved calcium-binding capacity

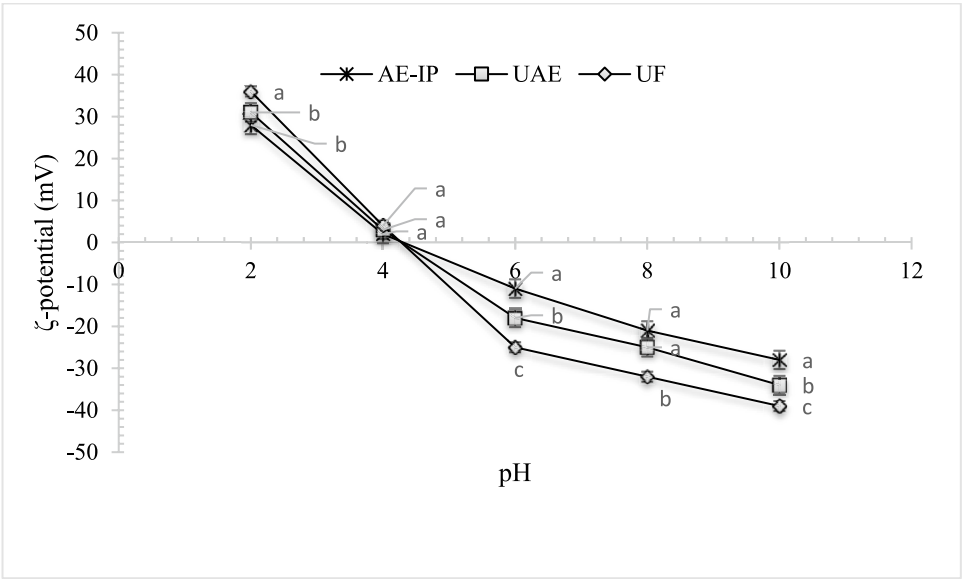

Fig. 2 ζ-potential of *S. scabrum* protein concentrates. Different lowercase letters indicate significant differences ($p < 0.05$) among extraction methods at the same pH

(Bocarando-Guzmán et al., 2022; Lu et al., 2010). UAE_SPC again showed intermediate sensitivity, while AE-IP_SPC required the highest Ca^{2+} concentration (11.15%), likely due to aggregation limiting accessible binding sites (Lu et al., 2010).

Water release after coagulation followed a similar trend. AE-IP_SPC gels exhibited the highest syneresis (46.71%), indicating weak and poorly interconnected networks. UAE_SPC demonstrated intermediate behavior. UF_SPC gels showed the lowest water release (15.42%), suggesting formation of a compact and continuous protein matrix with superior water-holding capacity. As such, milder extraction via ultrafiltration preserved structural integrity, resulting in greater thermal stability, enhanced calcium responsiveness, and improved gel water retention. In contrast, alkaline extraction promoted premature aggregation and weaker gel networks. These findings highlight the critical role of extraction method in governing gelation performance and functional application potential.

Results are expressed as mean ± standard deviation (n = 3) and means with different superscripts in the same row are significantly ($p < 0.05$) different. AE-IP_SPC: alkaline extraction-isoelectric precipitation, UAE_SPC: ultrasound-assisted extraction, and UF_SPC: ultrafiltration.

Flowability and Packing Properties

The flowability and packing characteristics of AE-IP_SPC, UAE_SPC and UF_SPC are summarized in Table 5. Significant differences ($p < 0.05$) were observed among extraction methods for bulk density, tapped density, Carr's compressibility index, Hausner ratio, and angle of repose, highlighting the influence of processing on powder behavior (Mochahary et al., 2022). As tapping reduces void spaces, tapped density values were consistently higher than bulk density, providing insight into particle arrangement and flow properties (Awari et al., 2025). These metrics are critical for evaluating powder performance in food and pharmaceutical formulations (Etti, 2020).

UF_SPC exhibited the highest bulk and tapped densities (0.48 and 0.59 g cm^{-3}), followed by UAE_SPC (0.43 and 0.55 g cm^{-3}), with AE-IP_SPC showing the lowest values (0.34 and 0.48 g cm^{-3}) (Table 5). The denser packing observed for UF_SPC is consistent with its smoother and more uniform particle morphology, whereas AE-IP_SPC displayed more aggregated microstructures (Fig. 3). Such microstructural differences are known to influence interparticle interactions and, consequently, powder flow. Aggregated or irregular particles typically show greater interparticle cohesion and friction, leading to poorer flowability, while more uniform, less aggregated particles tend to flow better (Awari et al., 2025; Etti, 2020).**Fig. 3** SEM micrographs *S. scabrum* leaf powder and protein concentrate at 3000×, 6000× and 10,000× magnification. SLP: *S. scabrum* leaf powder prior to extraction, AE-IP_SPC: alkaline extraction followed by isoelectric precipitation, UAE_SPC: ultrasound-assisted extraction, UF_SPC: ultrafiltration

These structural trends were mirrored in the compressibility metrics. AE-IP_SPC showed the poorest flow with Carr's index: 28.61% and Hausner ratio: 1.41, consistent with higher cohesion and friction as well as larger angles of repose reported for AE-IP-type powders (Awari et al., 2025; Tanyitiku & Njombissie Petcheu, 2025). UAE_SPC demonstrated intermediate (passable) flowability, with Carr's index: 20.41% and Hausner ratio: 1.28, alongside a reduced angle of repose (34.51°). The improvement of UAE_SPC relative to AE-IP_SPC is attributable to ultrasound-induced fragmentation and particle-size reduction, which promote particle uniformity and reduce mechanical interlocking and cohesive contacts (Maag et al., 2025; Pakawan, 2022). Notably, UF_SPC exhibited the most favorable flow properties (fair to good), with Carr's index: 18.71%, Hausner ratio: 1.22 and angle of repose: 30.67°. This could be attributed to mild membrane-based processing that preserves surface characteristics (minimizing denaturation-related tackiness) and yields more uniform particles with lower effective contact area per particle, thereby reducing cohesion and facilitating rearrangement under shear.

From an industrial perspective, the improved flow characteristics of UAE_SPC and especially UF_SPC indicate greater suitability for dry handling steps where uniform mixing, rapid rehydration, and automated dosing/transport are critical, for instance, protein-enriched beverages, dry blends, and bakery premixes (Awari et al., 2025). In contrast, AE-IP_SPC may require flow aids, granulation, or surface modification to achieve comparable processability.

Results are expressed as mean ± standard deviation (n = 3) and means with different superscripts in the same row are significantly ($p < 0.05$) different. AE-IP_SPC: alkaline extraction-isoelectric precipitation, UAE_SPC: ultrasound-assisted extraction, and UF_SPC: ultrafiltration.

Zeta Potential, Particle Size Distribution and Colloidal Stability

Zeta potential reflects the electrostatic charge on particle surfaces, which is critical for aggregation and helps maintain colloidal stability (Acar et al., 2025). Across all samples, zeta potential shifted from positive values at acidic pH to negative values under alkaline conditions (Fig. 2). At pH 2, all protein concentrates exhibited high positive zeta potential values (+21 to +36 mV), with no significant ($p > 0.05$) differences between AE-IP_SPC and UAE_SPC protein concentrates. All samples approached neutrality at pH 4–5 ($p > 0.05$), corresponding to the apparent isoelectric region where electrostatic repulsion is minimized and aggregation is favored (Zhang et al., 2024; Zheng et al., 2019). At

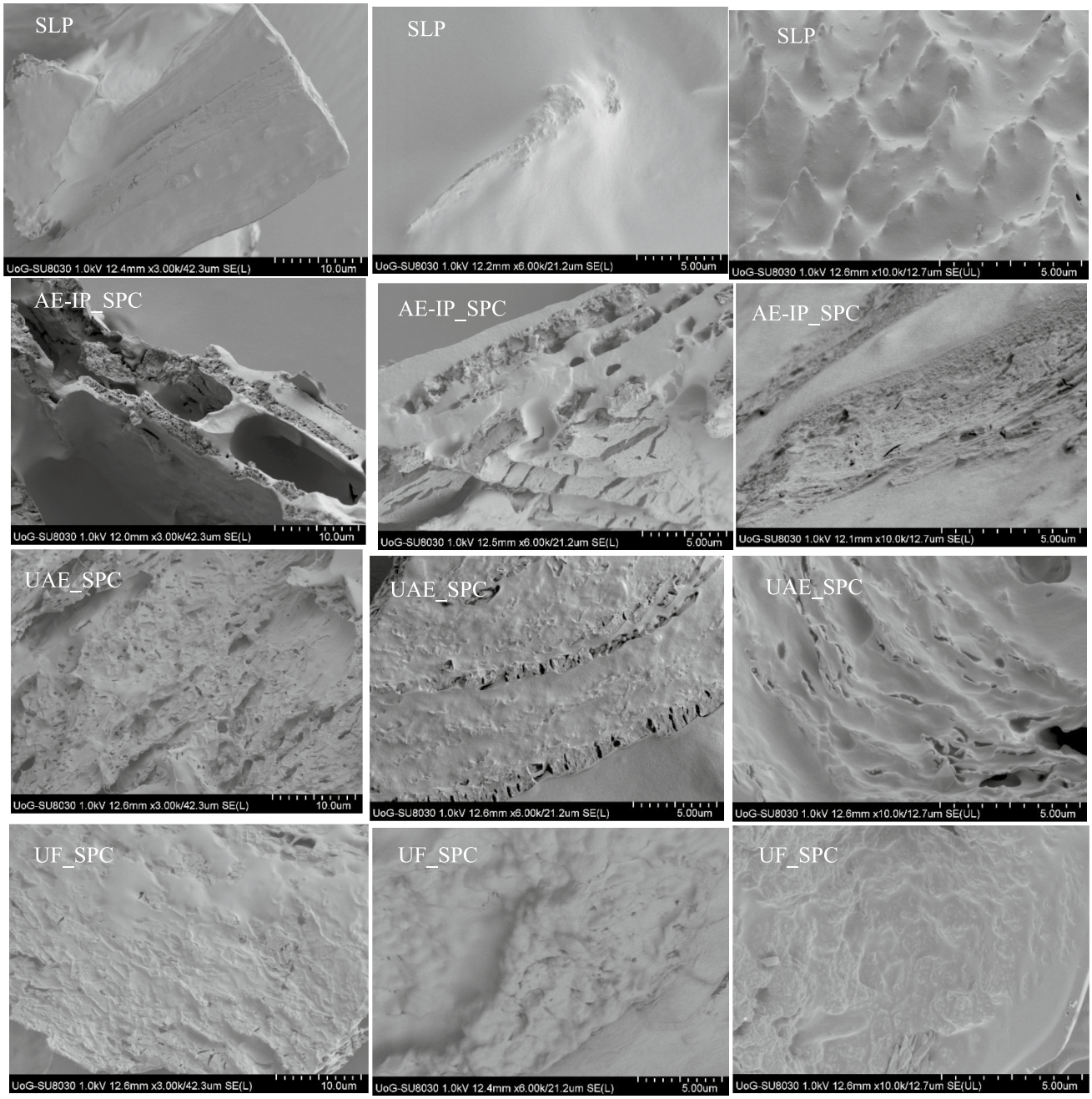

Fig. 3 SEM micrographs *S. scabrum* leaf powder and protein concentrate at 3000×, 6000×and 10,000×magnification. SLP: *S. scabrum* leaf powder prior to extraction, AE-IP_SPC: alkaline extraction followed by isoelectric precipitation, UAE_SPC: ultrasound-assisted extraction, UF_SPC: ultrafiltration

neutral and alkaline pH, UF_SPC exhibited the most negative zeta potential values (at −39 mV at pH 10), followed by UAE_SPC (−34 mV) and AE-IP_SPC (−28 mV), indicating superior electrostatic stabilization for membrane- and ultrasound-processed proteins. The lower absolute zeta potential observed for AE-IP_SPC may reflect irreversible aggregation and shielding of charged residues induced during alkaline solubilization and acid precipitation, a phenomenon widely reported for isoelectrically precipitated plant proteins (Illingworth et al., 2024). This reduced surface charge is consistent with extensive aggregation caused by pH-induced denaturation and precipitation (Bocarando-Guzmán et al., 2022). The superior electrostatic stability of UF_SPC and UAE_SPC aligns with their higher solubility, and improved emulsifying performance (Table 4). Ultrafiltration preserved more accessible ionizable groups by avoiding extreme pH

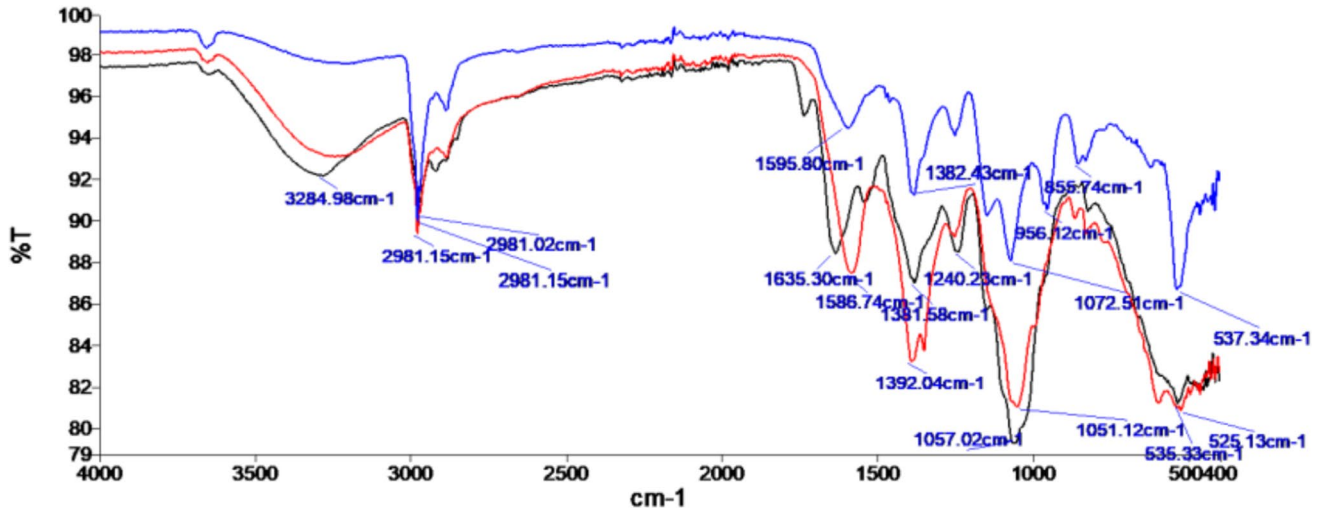

Fig. 4 FTIR spectra (4000–400 cm^{-1}) of *S. scabrum* protein concentrates obtained by different processing methods: AE-IP_SPC (alkaline extraction followed by isoelectric precipitation, blue), UAE_SPC (ultrasound-assisted extraction, red), and UF_SPC (ultrafiltration, black). Major absorption bands corresponding to protein functional groups are indicated

exposure, while ultrasound treatment partially enhanced surface charge through cavitation-induced structural disruption. Similar behavior has been reported for other leafy and legume protein systems, including pulses (Ma et al., 2022) sunflower (Huang et al., 2024) and other green leaf protein concentrates (Acar et al., 2025).

Particle size distribution showed a similar trend (Table 6). AE-IP_SPC exhibited the largest hydrodynamic diameter (28,653 nm) and highest PDI (0.53 ± 0.05), indicating extensive aggregation/flocs, consistent with protein clustering during isoelectric precipitation, whereas UF_SPC displayed the smallest particle size (1,994 nm) and lowest PDI (0.22 ± 0.08), suggesting limited aggregation and greater dispersion homogeneity. UAE_SPC showed intermediate particle size (6,716 nm), consistent with partial structural disruption without severe denaturation. Similar trends have been reported for soy proteins, where ultrasound treatment initially reduced particle size from 94.64 ± 3.91 µm to 63.71 ± 7.60 µm before prolonged exposure induced re-aggregation (Zheng et al., 2019). Conversely, Huang et al. (2024) reported far smaller average particle size (91.97 nm) for ultrafiltered sunflower protein compared to alkaline-extracted proteins (126.10 nm). This could be attributed to selective retention of protein molecules and removal of low-molecular-weight components that may otherwise promote aggregation (Khan et al., 2024; Maag et al., 2025).

Particle size strongly influences colloidal stability: smaller particles settle more slowly under gravity and diffuse more rapidly via Brownian motion, promoting uniform suspension (Acar et al., 2025). Typical interpretation for PDI include ~ 0.1: very monodisperse, 0.1–0.3: relatively narrow, 0.3–0.5: moderately broad and > 0.5: very polydisperse. As such, UF_SPC indicated fairly uniform, UAE_SPC moderately polydisperse, and AE-IP_SPC quite polydisperse. However, very fine particles present a larger surface area, increasing collision frequency and aggregation risk if not stabilized by electrostatic or steric mechanisms (Acar et al., 2025). Smaller particle size and higher absolute zeta potential in UF_SPC and UAE_SPC contribute to enhanced colloidal stability by promoting electrostatic repulsion and reducing sedimentation. These findings demonstrate that milder extraction approaches (UF and UAE) better preserved surface charge and limited aggregation, resulting in improved colloidal stability and superior interfacial functionality compared to conventional alkaline extraction.

Results are expressed as mean ± standard deviation (n = 3) and means with different superscripts in the same row are significantly ($p < 0.05$) different. AE-IP_SPC: alkaline extraction-isoelectric precipitation, UAE_SPC: ultrasound-assisted extraction, and UF_SPC: ultrafiltration.

SEM Micrographs

Morphological SEM micrographs of SLP, AE-IP_SPC, UAE_SPC and UF_SPC are presented in Fig. 3. SLP exhibited a rugged surface with pointed protrusions, characteristic of intact leaf tissue and native protein aggregates (Khan et al., 2024; Pérez-Vila et al., 2022). SEM imaging revealed distinct morphological features across the methods, with AE-IP_SPC exhibiting irregular, aggregated particles, while UAE_SPC and UF_SPC displayed finer, more dispersed structures. These structural differences are consistent with particle size data, where UF_SPC had the smallest hydrodynamic diameter and UAE_SPC an intermediate

profile. Smaller and more uniform aggregates increase the effective surface area available for interaction with water and oil, facilitating higher solubility and improved emulsifying activity, as observed for UF_SPC in Figs. 1 and 2. Zeta potential measurements further support this interpretation. At neutral and alkaline pH, both UAE_SPC and UF_SPC showed more negative surface charge than AE-IP_SPC, indicating a greater density of exposed ionizable groups. A more negative zeta potential enhances colloidal stability, which reduces aggregation in solution and promotes higher functional solubility. Increased electrostatic repulsion also favours the formation of smaller emulsion droplets, explaining the superior EAI of UAE_SPC relative to AE-IP_SPC (Table 4).

AE-IP_SPC displayed a dense, fibrous structure with irregular cracks, indicative of strong aggregation and structural collapse during precipitation. Similar compact morphologies have been reported for plant proteins extracted via pH-shifting techniques, where electrostatic neutralization promotes aggregation and collapse of protein networks (Illingworth et al., 2024; Pakawan, 2022). Such dense structures are generally associated with reduced hydration capacity and poor flowability, consistent with the lower water-holding capacity (Table 3) and inferior powder flow properties (Table 6) observed for AE-IP_SPC. In contrast, UAE_SPC exhibited smooth, layered structures with interconnected channels and cavities, suggesting cavitation-induced deagglomeration and improved openness. The presence of fissures and irregular cavities indicates that ultrasonic cavitation disrupted protein aggregates and weakened intermolecular interactions (Ragazzo-Calderón et al., 2024; Zheng et al., 2019). This porous morphology increases surface area and facilitates water penetration (Akyüz et al., 2025), explaining the enhanced solubility and hydration properties of UAE_SPC. Similar ultrasound-induced microstructural changes have been reported for sugar beet leaf proteins (Akyüz et al., 2025) and soy protein isolates (Qin et al., 2022; Zheng et al., 2019). UF_SPC was characterized by irregular wavy patterns and shallow depressions, suggesting moderate aggregation with porous regions. The absence of severe structural collapse reflects the mild processing conditions of ultrafiltration, which minimize protein denaturation and aggregation (Pakawan, 2022). This likely contributed to the improved solubility (Fig. 1) and powder flowability (Table 5) observed for UF_SPC.

FTIR spectral analysis

FTIR spectra (Fig. 4) provided complementary insights into protein secondary structures. All spectra exhibited a broad absorption band in the region of 3200–3400 cm^{-1}, attributed to O–H and N–H stretching vibrations, which are characteristic of hydrogen bonding in proteins and residual moisture. Minor shifts in band intensity were observed among samples, suggesting differences in hydrogen-bonding environments induced by processing conditions. Peaks around 2920–2850 cm^{-1} corresponded to C-H stretching of aliphatic side chains and lipid-associated moieties, with slightly higher intensity in AE-IP_SPC, likely reflecting residual non-protein components. Specifically, UF_SPC exhibited a pronounced absorption band at ~ 3284.98 cm^{-1}, corresponding to N–H and O–H stretching vibrations associated with hydrogen-bonded amide groups and protein-water interactions. The presence and higher intensity of this band in UF_SPC suggests superior retention of hydrogen bonding and a more native-like protein structure compared to AE-IP_SPC and UAE_SPC. Similar observations have been reported for mildly processed chickpea protein isolates (Yixiang Xu et al., 2017a, 2017b) and broccoli, black carrot, beetroot, and cauliflower leaf protein concentrates (Acar et al., 2025), where hydrogen bonding contributed to enhanced solubility and interfacial functionality. Moreover, this enhanced hydrogen bonding indicated by the 3259 cm^{-1} band aligns with the superior solubility, colloidal stability, and emulsifying performance observed for UF_SPC.

The amide I region (1600–1700 cm^{-1}), primarily associated with C = O stretching vibrations and commonly used to assess protein secondary structure, showed prominent bands near 1650–1660 cm^{-1} and 1638–1645 cm^{-1} in UF_SPC samples, corresponding to α-helical and β-sheet structures, respectively. UF_SPC displayed comparatively broader amide I bands than UAE_SPC and AE-IP_SPC, suggesting partial rearrangement of secondary structures induced by membrane-based fractionation. Partial unfolding increases the exposure of hydrophobic residues and flexible segments, which enhances water-protein and oil-protein interactions, thereby improving water holding capacity (WHC) and oil holding capacity (OHC). Similar broadening has been reported in membrane-processed plant proteins and is commonly attributed to disruption of non-covalent interactions and partial unfolding rather than chemical modification.

The amide II band (1540–1560 cm^{-1}), arising from N–H bending coupled with C-N stretching, was present in all spectra with comparable intensity, indicating that peptide backbone integrity was largely preserved regardless of extraction or concentration method. Likewise, the amide III region (1200–1350 cm^{-1}) exhibited overlapping contributions from α-helices, β-sheets, and random coils, with modest intensity differences suggesting subtle conformational variations rather than major structural transitions. The attenuation of the amide I region is likely due to overlap with other constituents such as polysaccharides, phenolic compounds, and mineral components, which are abundant in leafy matrices and contribute strong absorbance in adjacent regions (Acar et al., 2025; Muller et al., 2024). Similar

spectral patterns have been reported for protein concentrates from moringa leaves and soy, showing absorption bands in the 1540–1650 cm^{-1} region (amide II) and carbohydrate-associated bands between 1100–1800 cm^{-1} (Bocarando-Guzmán et al., 2022; Zheng et al., 2019). Likewise, Yixiang Xu et al., (2017a, 2017b) observed FTIR spectra of chickpea protein isolates with peaks at 1536 cm^{-1} (amide II: NH bending and CN stretching) and broad bands centered at 3300 cm^{-1} and 2950 cm^{-1} corresponding to -OH and -CH stretching. Acar et al. (2025) reported fat, carbohydrate, and protein peaks between 2800–3000 cm^{-1} in broccoli, black carrot, beetroot, and cauliflower leaf protein concentrates, while peaks between 3200–3600 cm^{-1} were attributed to water or carbohydrate presence.

In this study, differences in the intensity and shape of the amide II and III bands among the samples indicated variations in protein conformation and intermolecular interactions. AE-IP_SPC exhibited broader amide II bands, suggesting increased aggregation and reduced molecular mobility following alkaline treatment and isoelectric precipitation. In contrast, UAE_SPC showed moderate changes in band intensity, reflecting partial unfolding induced by ultrasonic cavitation. UF_SPC displayed comparatively sharper amide II and III bands, indicating better preservation of protein conformation under mild processing conditions.

In the fingerprint region below 1200 cm^{-1}, bands associated with C–O, C–C, and C–N stretching vibrations were observed. AE-IP_SPC showed slightly stronger absorptions in this region, which may be related to greater retention of carbohydrate-associated and phenolic components, consistent with its higher fiber and ash contents reported in Table 1. In contrast, UAE_SPC and UF_SPC exhibited comparatively smoother baseline features, reflecting the removal of low-molecular-weight non-protein constituents during sonication and membrane filtration.

Overall, the FTIR spectra demonstrate that while all *S. scabrum* protein concentrates retained the characteristic functional groups of plant proteins, the extraction method influenced band intensity and broadening, particularly within the amide I region. Alkaline extraction revealed more intense O–H, C-O, and carbohydrate fingerprint bands indicating higher polysaccharide, moisture, and polyphenolic content. Ultrasonication and ultrafiltration showed stronger Amide I (~ 1635 cm^{-1}) and Amide II (~ 1590 cm^{-1}) peaks indicating higher protein content and dominant β-sheet structure, reduced carbohydrate fingerprint bands that confirms effective removal of cell wall polysaccharides. In addition, they induced mild conformational rearrangements without evidence of protein degradation, supporting their suitability as alternative processing strategies for producing structurally intact protein concentrates.

Conclusion

This study highlights the potential of *Solanum scabrum* protein concentrates as sustainable, plant-based ingredients, whose functional properties can be tailored through the choice of recovery strategy. AE-IP promoted aggregation with reduced functional properties. In contrast, UAE enhanced protein recovery while partially preserving functional performance, whereas UF produced concentrates with superior solubility, emulsifying and foaming stability, flowability, and structural integrity, despite lower yields. From an application perspective, UF- and UAE-derived protein concentrates show strong potential for incorporation into emulsified foods, beverages, foamed systems, and powdered formulations, where high solubility, interfacial stability, and good handling properties are critical. Although UF is not an extraction method per se, its mild, solvent-free separation mechanism highlights its promise as a downstream purification strategy for producing high-quality leaf protein ingredients. However, this study was conducted at laboratory scale, and the relatively lower yield observed for UF highlights a key trade-off between protein recovery and functional quality that can be addressed during process optimization. The main limitations of this study include the absence of pilot-scale validation, sensory evaluation, and long-term storage stability assessment. Future research should therefore focus on techno-economic and life-cycle assessments to fully establish the industrial feasibility and sustainability of *S. scabrum* leaf protein. Nonetheless, this work provides mechanistic and practical insights into how extraction and recovery strategies shape the functionality of leaf-derived proteins and supports the development of *S. scabrum* as a viable, underutilized protein source for sustainable plant-based food systems.

Acknowledgements The authors thank Dr. Igor Casimir Njombissie Petcheu for providing Solanum scabrum during the preliminary stages of this research.

Authors Contribution **Mary Nkongho Tanyitiku**: Conceptualization, Methodology, Investigation, Formal analysis, Funding acquisition, Supervision, Writing—original draft, Writing—review & editing. **Shiksha Chaturvedi**: Conceptualization, Methodology, Data curation, Writing—review & editing **Rakshya Pandit**: Conceptualization, Validation, Writing—review & editing. **Komalpreet**: Conceptualization, Formal analysis, Writing – review & editing. **Jyothi Dasari**: Conceptualization, Formal analysis, Writing—review & editing. **Aparna Philipose Antony**: Conceptualization, Methodology, Data curation, Validation, Writing—review & editing.

Funding This research did not receive any specific grant from funding agencies in the public, commercial, or not-for-profit sectors.

Data Availability Data will be made available on request

Declarations

Competing interest The authors declare that they have no known competing financial interests or personal relationships that could have appeared to influence the work reported in this paper.

The authors declare no competing interests.

References

Acar, E. G., Ozen, E., Dikmetas, D. N., Alakaş, E., Karbancioglu-Guler, F., Esatbeyoglu, T., ..., Kahveci, D. (2025). Protein extraction from agricultural waste. Effects of the precipitation method on the composition and physicochemical properties of green leaf protein concentrates. *90*(9). https://doi.org/10.1111/1750-3841.70563

Akyüz, A., Tekin, İ, Aksoy Caf, Z., & Ersus, S. (2025). Sustainable protein extraction from sugar beet leaves: A comparative study of combined techniques and structural properties. *Sugar Tech*. https://doi.org/10.1007/s12355-025-01657-4

Anuar, M. N. B., & Zuo, J. (2025). Enhancing yellow pea protein extraction and purification through ultrafiltration. *Membranes, 15*, Article 326. https://doi.org/10.3390/membranes15110326

Awari, A., Kaushik, D., Öz, E., Proestos, C., Brennan, C., Oz, F., & Kumar, M. (2025). Study on *Commiphora mukul* (Guggul) gum: Exploring the proximate composition and techno-functional properties and efficacy against obesity. *International Journal of Food Science and Technology, 60*. https://doi.org/10.1093/ijfood/vvaf157

Bando, C. D., Ikwebe, J., Gambo, S. U., Efi, U. J., Jonathan, A. P., Adamu, N. T., Danjuma, S., & Okonofua, E. P. (2025). Comparative analysis of the nutritional composition of hukleberry (*Solanum scabrum*) and spinach (*Amaranthus hybridus*). *SSR J Med Sci, 2*(2), 41–51.

Bayang, J. P., Touwang, C., Mamoudou, H., Woudam, E. S., & Koubala, B. B. (2025). Variation of nutrients and bioactive compounds of five wild edible leafy vegetables from Far North region of Cameroon. *Food Chemistry Advances, 6*, Article 100849. https://doi.org/10.1016/j.focha.2024.100849

Bocarando-Guzmán, M. D., Luna-Suárez, S., Hernández-Cázares, A. S., Herrera-Corredor, J. A., Hidalgo-Contreras, J. V., & Ríos-Corripio, M. A. (2022). Comparison of the physicochemical and functional properties of flour and protein isolate from moringa (*Moringa oleifera* Lam.) leaves. *International Journal of Food Properties, 25*(1), 733–747. https://doi.org/10.1080/10942912.2022.2058533

Cheng, F., Guowei, S., Chen, L., Dai, C., Wan, H., Chen, H., & Dong, X. (2021). Ultrasound-microwave assisted extraction of proteins from *Moringa oleifera* leaves: Comparative optimization study and LC-MS analysis of the protein concentrate. *Journal of Food Processing and Preservation, 45*. https://doi.org/10.1111/jfpp.15547

Cruz-Solis, I., Ibarra-Herrera, C. C., Rocha-Pizaña, M. D. R., Luna-Vital, D. (2023). Alkaline Extraction-Isoelectric Precipitation of plant proteins. In: A. J. Hernández-Álvarez, M. Mondor, M. G. Nosworthy (Eds.), *Green protein processing technologies from plants*. Springer, Cham. https://doi.org/10.1007/978-3-031-16968-7_1

Dirr, S., & Karslioglu, Ö. Ö. (2024). Impact of various extraction technologies on protein and chlorophyll yield from stinging nettle. *Foods, 13*(20). https://doi.org/10.3390/foods13203318

Etti, C. (2020). Physical, Proximate and toxicological properties of *Andrographis paniculata* herbal powder beverage mix. *International Journal of Food Science, Nutrition and Dietetics*, 448–454. https://doi.org/10.19070/2326-3350-2000080

FAO/WHO/UNU. (2007). *Expert consultation on protein and amino acid requirements in human nutrition. Protein and amino acid requirements in human nutrition: report of a joint FAO/WHO/UNU expert consultation*. World Health Organization. https://iris.who.int/handle/10665/43411. Accessed 8 Aug 2025.

Furia, K. A., Majzoobi, M., Torley, P. J., & Farahnaky, A. (2025). Innovative approaches in leaf protein extraction: Advancements, challenges, and applications in sustainable food formulation and design. *Critical Reviews in Food Science and Nutrition*. https://doi.org/10.1080/10408398.2025.2542516

Gasparre, N., Rosell, C. M., & Boukid, F. (2025). Enzymatic hydrolysis of plant proteins: Tailoring characteristics, enhancing functionality, and expanding applications in the food industry. *Food and Bioprocess Technology, 18*(4), 3272–3287. https://doi.org/10.1007/s11947-024-03648-x

Hojilla-Evangelista, M. P., Selling, G. W., Hatfield, R., & Digman, M. (2017). Extraction, composition, and functional properties of dried alfalfa (*Medicago sativa* L.) leaf protein. *Journal of the Science of Food and Agriculture, 97*(3), 882–888. https://doi.org/10.1002/jsfa.7810

Huang, X., Li, Y., Cui, C., & Sun-Waterhouse, D. (2024). Structural, functional properties, and in vitro digestibility of sunflower protein concentrate as affected by extraction method: Isoelectric precipitation vs ultrafiltration. *Food Chemistry, 439*, Article 138090.

Illingworth, K. A., Lee, Y. Y., & Siow, L. F. (2024). Functional properties of *Moringa Oleifera* protein isolates as influenced by different isolation techniques, pH, and ionic strength. *Food and Bioprocess Technology, 17*(10), 3060–3073. https://doi.org/10.1007/s11947-023-03279-8

Ismail, B. P., Senaratne-Lenagala, L., Stube, A., & Brackenridge, A. (2020). Protein demand: Review of plant and animal proteins used in alternative protein product development and production. *Animal Frontiers, 10*(4), 53–63. https://doi.org/10.1093/af/vfaa040

John, H., Giri, S., Subeesh, A., Chandra, P., & Pandiselvam, R. (2024). Optimization of process parameters for the production of soy protein by ultrafiltration using ANN. *Journal of Food Processing and Preservation, 2024*, 1–10. https://doi.org/10.1155/2024/5535413

Kadam, S. U., Tiwari, B. K., Álvarez, C., & O'Donnell, C. P. (2015). Ultrasound applications for the extraction, identification and delivery of food proteins and bioactive peptides. *Trends in Food Science & Technology, 46*(1), 60–67. https://doi.org/10.1016/j.tifs.2015.07.012

Kavle, R. R., Pritchard, E. T. M., Carne, A., Bekhit, A.E.-D.A., Morton, J. D., & Agyei, D. (2023). Nutritional composition and techno-functional properties of sago palm weevil (*Rhynchophorus ferrugineus*) larvae protein extract. *Journal of Asia-Pacific Entomology, 26*(2), 102086. https://doi.org/10.1016/j.aspen.2023.102086

Khan, M. K., Mazhar, H., Shehzadi, U., Ahmad, M. H., Nadeem, M. T., Ahmad, R. S., ..., Mukonzo, E. L. (2024). The effect of ultrasound-assisted extraction process on techno-functional properties of protein from *Moringa oleifera* leaves. *Cogent Food & Agriculture,10*(1), Article 2436645. https://doi.org/10.1080/23311932.2024.2436645.

Kirigia, D., Winkelmann, T., Kasili, R., & Mibus, H. (2019). Nutritional composition in African nightshade (*Solanum scabrum*) influenced by harvesting methods, age and storage conditions. *Postharvest Biology and Technology, 153*, 142–151. https://doi.org/10.1016/j.postharvbio.2019.03.019

Ladjal-Ettoumi, Y., Boudries, H., Chibane, & M. Romero, A. (2016). Pea, chickpea and lentilprotein isolates: Physicochemical

characterization and emulsifying properties. *Food Biophysics, 11*, 43–51. https://doi.org/10.1007/s11483-015-9411-6

Leffler, T. P., Moser, C. R., McManus, B. J., Urh, J. J., Keeton, J. T., Claflin, A., Adkins, K., Claflin, A., Davis, C., Elliot, J., Goin, P., Horn, C., Humphries, J., Ketteler, K., Perez, P., & Steiner, G. (2008). Determination of moisture and fat in meats by microwave and nuclear magnetic resonance analysis: Collaborative study. *Journal of AOAC International, 91*(4), 802–810. https://doi.org/10.1093/jaoac/91.4.802.

Lu, X., Lu, Z., Yin, L., Cheng, Y., & Li, L. (2010). Effect of preheating temperature and calcium ions on the properties of cold-set soybean protein gel. *Food Research International, 43*(6), 1673–1683. https://doi.org/10.1016/j.foodres.2010.05.011

Lugumira, R., Tafiire, H., Vancoillie, F., Ssepuuya, G., & Van Loey, A. (2025). Nutrient and phytochemical composition of nine African leafy vegetables: A comparative study. *Foods, 14*(8). https://doi.org/10.3390/foods14081304

Ma, K. K., Grossmann, L., Nolden, A. A., McClements, D. J., & Kinchla, A. J. (2022). Functional and physical properties of commercial pulse proteins compared to soy derived protein. *Future Foods, 6*, Article 100155. https://doi.org/10.1016/j.fufo.2022.100155

Maag, P., Cutroneo, S., Tedeschi, T., Grüner-Lempart, S., Rauh, C., & Karslioglu, Ö. Ö. (2025). Optimization of protein extraction from duckweed using different extraction processes. *Food and Bioprocess Technology, 18*(6), 5510–5531. https://doi.org/10.1007/s11947-025-03777-x

Mishyna, M., Martinez, J.-J.-I., Chen, J., & Benjamin, O. (2019). Extraction, characterization and functional properties of soluble proteins from edible grasshopper (*Schistocerca gregaria*) and honey bee (*Apis mellifera*). *Food Research International, 116*, 697–706.

Mochahary, B., Brahma, S., Kalita, M., & Goyal, A. (2022). Characterization of indigenous plants for herbal formulations preparation based on pharmacognostic and physiochemical data. *Plant Science Today*. https://doi.org/10.14719/pst.1709

Muller, T., Bernier, M. -È., & Bazinet, L. (2024). Optimization of water lentil (duckweed) leaf protein purification: Identification, structure, and foaming properties. *Foods, 12*(18), 3424. https://doi.org/10.3390/foods12183424

Njong, C. E., Dibanda, F. R., & Ejoh, R. A. (2023). Recipes and proximate composition of some traditional African nightshade dishes consumed in the North West region of Cameroon. *Journal of Food Sciences, 4*, 12–34. https://doi.org/10.47941/jfs.1198

Odongo, G. A., Schlotz, N., Baldermann, S., Neugart, S., Huyskens-Keil, S., Ngwene, B., Trierweiler, B., Schreiner, M., & Lamy, E. (2021). African nightshade (*Solanum scabrum* Mill.): Impact of cultivation and plant processing on its health promoting potential as determined in a human liver cell model. *Nutrients, 10*, 1532. https://doi.org/10.25932/publishup-45911

Pakawan, M. (2022). *Physico-chemical and functional properties of leaf protein concentrates isolated using different techniques : A thesis presented in partial fulfilment of the requirements for the degree of Master of Food Technology at Massey University, Riddet Institute, Palmerston North, New Zealand*. Submitted July 2022. p. 155. Available at: https://mro.massey.ac.nz/handle/10179/69314. Accessed 13 Sept 2025.

Pérez-Vila, S., Fenelon, M., Hennessy, D., O'Mahony, J. A., & Gómez-Mascaraque, L. G. (2024). Impact of the extraction method on the composition and solubility of leaf protein concentrates from perennial ryegrass (*Lolium perenne* L.). *Food Hydrocolloids, 147*, Article 109372. https://doi.org/10.1016/j.foodhyd.2023.109372

Pérez-Vila, S., Fenelon, M. A., O'Mahony, J. A., & Gómez-Mascaraque, L. G. (2022). Extraction of plant protein from green leaves: Biomass composition and processing considerations. *Food Hydrocolloids, 133*, Article 107902. https://doi.org/10.1016/j.foodhyd.2022.107902

Qin, P., Wang, T., & Luo, Y. (2022). A review on plant-based proteins from soybean: Health benefits and soy product development. *Journal of Agriculture and Food Research, 7*, Article 100265. https://doi.org/10.1016/j.jafr.2021.100265

Ragazzo-Calderón, F. Z., Iñiguez-Moreno, M., Calderón-Santoyo, M., & Ragazzo-Sánchez, J. A. (2024). The structural modification of jackfruit leaf proteins (*Artocarpus heterophyllus* Lam.) by high-intensity ultrasound alters their techno-functional properties and antioxidant capacity. *Applied Sciences, 14*(18), Article 8301. https://doi.org/10.3390/app14188301

Rezvankhah, A., Yarmand, M. S., Ghanbarzadeh, B., & Mirzaee, H. (2021). Generation of bioactive peptides from lentil protein: Degree of hydrolysis, antioxidant activity, phenol content, ACE-inhibitory activity, molecular weight, sensory, and functional properties. *Journal of Food Measurement and Characterization, 15*(6), 5021–5035. https://doi.org/10.1007/s11694-021-01077-4

Tanyitiku, M. N., & Njombissie Petcheu, I. C. (2025). Technofunctional properties of stinging nettle (*Urtica dioica* L.) leaf flour and its enhancing pasting, physical and sensory characteristics in gluten-free rice waffles. *Journal of Food Quality*. https://doi.org/10.1155/jfq/9418554

Uddin, M., Ishizaki, S., & Tanaka, M. (2000). Coagulation test for-determining end-point temperature of heated blue marlin meat. *Fisheries Science, 66*, 153–160.

Vogelsang-O'Dwyer, M., Sahin, A. W., Bot, F., O'Mahony, J. A., Bez, J., Arendt, E. K., & Zannini, E. (2023). Enzymatic hydrolysis of lentil protein concentrate for modification of physicochemical and techno-functional properties. *European Food Research and Technology, 249*(3), 573–586. https://doi.org/10.1007/s00217-022-04152-2

Xu, Y., Li, Y., Bao, T., Zheng, X., Chen, W., & Wang, J. (2017). A recyclable protein resource derived from cauliflower by-products: Potential biological activities of protein hydrolysates. *Food Chemistry, 221*, 114–122. https://doi.org/10.1016/j.foodchem.2016.10.053

Xu, Y., Obielodan, M., Sismour, E., Arnett, A., Alzahrani, S., & Zhang, B. (2017). Physicochemical, functional, thermal and structural properties of isolated Kabuli chickpea proteins as affected by processing approaches. *International Journal of Food Science and Technology, 52*(5), 1147–1154. https://doi.org/10.1111/ijfs.13400

Yang, C., Liu, W., Zhu, X., Zhang, X., Wei, Y., Huang, J., Yang, F. Yang, F. (2024). Ultrasound-assisted enzymatic digestion for efficient extraction of proteins from quinoa. *LWT-Food Science and Technology, 194*. https://doi.org/10.1016/j.lwt.2024.115784.

Yao, S., Li, W., Martin, G. J. O., & Ashokkumar, M. (2023). An investigation into the mechanism of Alkaline Extraction-Isoelectric Point Precipitation (AE-IEP) of high-thiol plant proteins. *Applied Sciences, 13*, Article 6469. https://doi.org/10.3390/app13116469

Zhao, L., Cheng, X., Song, X., Ouyang, D., Wang, J., Wu, Q., & Jia, J. (2023). Ultrasonic assisted extraction of mulberry leaf protein: Kinetic model, structural and functional properties, in vitro digestion. *Process Biochemistry, 128*, 12–21. https://doi.org/10.1016/j.procbio.2023.02.014

Zhang, J., Ji, S., Liang, J., Chen, Y., Tang, W., & Lyu, F. (2024). Research progress and latest application of ultrasonic treatment on protein extraction and modification. *International Journal of Food Science and Technology, 59*(7), 4374–4392. https://doi.org/10.1111/ijfs.17196

Zheng, T., Li, X., Taha, A., Wei, Y., Hu, T., Fatamorgana, P. B., & Hu, H. (2019). Effect of high intensity ultrasound on the structure and physicochemical properties of soy protein isolates produced by different denaturation methods. *Food Hydrocolloids, 97*, Article 105216. https://doi.org/10.1016/j.foodhyd.2019.105216